

Computing with two quantum reservoirs connected via optimized two-qubit nonselective measurements.

Stephen Vintskevich^{1,*} and Dmitry Grigoriev^{1,2,*}

^{1,*}Moscow Institute of Physics and Technology, Institutskii Per. 9, Dolgoprudny, Moscow Region 141700, Russia

^{2,*}Bitronics NeuroLab, Likhachevskiy Proyezd 4, Dolgoprudny, Moscow Region 141701, Russia

*vintskevich@phystech.edu

ABSTRACT

At the present level of technology, quantum reservoir computing is one of the most promising and experimentally available techniques of hybrid quantum-classical machine learning. However, quantum reservoirs' practical applications are limited due to technological restrictions in the size of quantum systems, issues with gates control, and the affection of noise. Here we proposed a novel approach to connect quantum reservoirs in a network to overcome these issues and enhance quantum reservoir computing performance. This approach is based on an optimized two-qubit nonselective measurements channel. We also introduce an optimized single qubit purification channel for further quantum reservoir computing enhancements. We validate our approach via numerical simulations. We demonstrate that the optimized channels applied to a seven-qubits network can effectively transfer information between its parts. The resulting overall performance is comparable with networks of twenty-five qubits in total connected via a classical information link.

Introduction

In the seminal paper¹, the authors proposed utilizing complex dynamics of multipartite quantum systems - quantum reservoirs (QR) to perform learning and computational tasks with time-dependent data. This approach was named Quantum Reservoir Computing (QRC) as a counterpart to classical Reservoir Computing (RC) - a powerful framework that stems from recurrent neural network theory (see work² and references therein). Formally, the components of QRC can be divided into four main parts. The first valuable information is encoded in a state of some quantum system - orange arrow in and blocks marked by symbol Φ_e Fig.(1) - (a). It is then processed and transformed via dynamics of a QR - blocks with symbol marked by \mathcal{U}_R in Fig.(1) - (a,c) represents unitary evolution. The third is performing measurements of some quantum observable to gather processed encoded information (also named output signal). Finally, these output signals - measurements results are used to train a simple linear model. The detailed QRC framework is depicted in Fig. (1). To implement QRC in practice, one usually operates with a huge ensemble of identically prepared quantum systems (see Fig. 1 - (a)) to effectively perform measurements using multiple copies of a system. As a physical realization of an ensemble, one can utilize nuclear magnetic resonance (NMR) spin systems³⁻⁶, semiconducting quantum dots⁷, superconducting qubits⁸ and bosonic networks^{9,10}. The great potential and scope of QRC have been recently demonstrated not only for processing classical temporal signals but also for quantum state preparation¹¹ and reconstruction¹², training of an entanglement witness operator¹³, and quantum tomography¹⁴.

In contrast to other developing methods, such as quantum neural networks¹⁵, quantum circuit learning^{16,17}, and quantum machine learning^{18,19}, intrinsic parameters of QRs and their dynamics are usually assumed to be fixed and non-tunable. However, it is important to emphasize recently were presented methods of enhancements and adjustments, such as boosting QR's computational power through spatial multiplexing technique²⁰ and analyzing QR's intrinsic dynamics for better performance²¹. The latter is similar to hyperparameter tuning in neural networks training. It should be noted a recent approach that addresses the scalability and efficiency of QRC is called High Order Reservoir Computing. (HQRC²²). The mentioned adjustments and enhancements with multiple small QRs are essential for realistic experimental implementations of QRC based on modern quantum technology²³. Additionally, QRC may be interpreted as the 'inverse' to recently proposed methods that apply machine learning techniques to learn non-Markovian quantum dynamics of a qubit system in a complex environment^{24,25}.

In this work, we concentrate on further developing an idea of constructing small networks of multiple QRs. We propose a novel approach based on an action of a quantum channel that creates correlation and information transfer between two QRs. A quantum channel is a completely positive, trace-preserving linear map (CPTP) on a set of trace class operators that acts on some Hilbert space²⁶. For simplicity, we named this channel a *bridge*.

To implement the bridge channel, we perform two-qubit nonselective projective measurements (measurements without reading the outcome) along a two-qubit basis. As it was pointed out in work²⁷, nonselective measurements can transfer

information and, as we demonstrated, can be used to improve QRC. One of the most vivid properties of multipartite quantum systems - entanglement must be presented on a particular measurement basis to transfer information between different QRs. However, the presence of entanglement in a measurement basis is not sufficient for the acceptable performance of QRC with the bridge channel. Interestingly, it was proven²⁸ that nonselective projective measurement might even entangle two initially disentangled qubit subsystems, but the result substantially depends on a chosen basis. It was also pointed out²⁸ that projective nonselective measurements along a maximally entangling basis are useless for any entanglement gain between arbitrary two-qubit subsystems. Even if the measurement basis is entangled, it does not guarantee good QRC performance. To resolve this issue, we suggest a heuristic method to numerically optimize bridge's parameters with the help of the Adam optimizer, which is commonly used in machine learning²⁹. Our optimization method does not depend on a particular task or encoded information in QRs and can be considered as an adjustment to QRs' dynamics.

We also added auxiliary purification channels to act on bridge's qubits, which proved useful for even better performance. We utilize the same ansatz that we are using for the bridge optimization but with a slightly different heuristic to optimize this auxiliary purification channel. Details are presented in the **Methods** section. To demonstrate QRC assisted by bridge and purification channels we numerically simulate the performance of our QRs. In these simulations we are analyzing standard metrics for short-term memory tasks (STM)²¹, which gives us an understanding of the memory capability of QRs, one of the essential characteristics for successful QRC¹. To demonstrate performance with the bridge channel, we consider a setup where two QRs are connected only via the bridge. We assume that all valuable information is encoded in a single qubit of QR-*A* named encoding qubit. An output signal is obtained via measurements both on a subsystem of QR-*B* and also on a full QR system. Finally, we discuss possible new avenues in research and comparison with other setups (e.g., HQRC²²).

Results

General framework.

In this subsection we provided an outline of a standard QRC framework. Its schematic is depicted on Fig. 1. We considered a

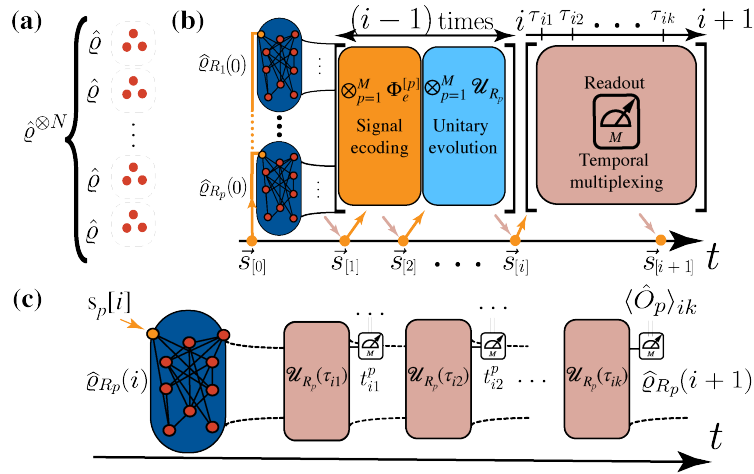


Figure 1. The schematic of a general QRC framework. **(a)** - Physical realization. In practice, one prepares identical physical systems (spins, atoms, etc.) using similar initial conditions. Signal encoding procedures and measurements are performed on each subsystem to get output signals - ensemble mean value of a given observable. **(b)** - Dynamics of a QRC framework. An initial joint state of all QRs is factorized $\hat{\rho}[i] = \otimes_{p=1}^M \hat{\rho}_{R_p}[i], p = 1, \dots, M$; for $i-1$ steps the dynamics of each QR are governed by the alternation of encoding- $\Phi_e^{[p]}[\bullet]$ and the unitary evolution- \mathcal{U}_{R_p} channels followed by the output signal readout step. The input signal \bar{s}_i (orange arrows) at timestep i can be mixed with QRs' output signals (beige arrows) at timestep $i-1$, Eq. (2) **(c)** - readout step with temporal multiplexing. Time interval $[i, i+1], \forall i \in [1, i_{max}]$ is split into K smaller sub-intervals τ_{ik} for each reservoir. For each timestep $t_{ik}^p = t_{i+(k/K)}^p$ one performs measurements to extract output signal $\langle \hat{O}_p \rangle_{ik}$. Usually, one does not take into account the backaction of measurements on QRs' dynamics. Thus, it is implied that one must repeat all the operations applied on QRs preceding timestep t_{ik}^p . Note that for various p , the observables $\langle \hat{O}_p \rangle_{ik}$ and times t_{ik}^p might be different.

model of multiple reservoirs $R_p, p = 1, \dots, M$ with similar structures, each consisting of n_p qubits.

A quantum state of a particular QR at the timestep i is described by the positive Hermitian density operator $\hat{\rho}_p[i]$ with the unit trace $\text{tr}(\hat{\rho}_p[i]) = 1, \forall i$. In the case of multiple reservoirs, we assume that all reservoirs are completely uncorrelated

at an initial time: $\hat{\rho}[i] = \otimes_{p=1}^M \hat{\rho}_p[i]$. The unitary evolution dynamics of each QR is governed by a fully connected Ising-type Hamiltonian $\hat{H}_{R_p} = \sum J_{ij}^{[p]} \hat{X}_i \hat{X}_j + h_i^p \hat{Z}_i$, (where \hat{X}, \hat{Z} are Pauli operators). In general QRC approach one operates with a classical discretized temporal signal $\vec{s}(t) \rightarrow \vec{s}[i]$. An encoding procedure is performed via a set of quantum channels:

$$\{\Phi_e^{[p]}\} : \Phi_e^{[p]}[\hat{\rho}] = \hat{\rho}_{(\bullet_p)}(\vec{s}[i]) \otimes \text{tr}_{(\bullet_p)}(\hat{\rho}). \quad (1)$$

Channels in Eq.(1) map the initial state of the overall QR system into a tensor product of states correspond to two subsystems. Encoding subsystems state (denoted as \bullet_p) is carrying valuable information about the signal, while $\text{tr}_{(\bullet_p)}(\hat{\rho})$ is a state of other QR's subsystems. Symbol $\text{tr}_{(\bullet_p)}$ denotes partial trace operation. Thus the subsequent application of encoding and evolution channels maps this valuable information from the input signal to a $4^{N_{total}}$ -dimensional vector in the real space of a trace class operators. We denote $N_{total} = \sum_{p=1}^M n_p$ to be the total number of qubits in the QR system. We preserve the same signal structure that was used in the works. In principle, one can mix signals' inputs at particular timesteps and the outputs from different QRs (HQRC) on a previous timestep^{20,22}. For instance, in the case of two QRs, the mixture of input and output signals at timestep i is given by:

$$\vec{s}'[i] = \begin{pmatrix} s'_A[i] \\ s'_B[i] \end{pmatrix} = \alpha \begin{pmatrix} s_A[i] \\ s_B[i] \end{pmatrix} + (1 - \alpha) W_{mix}^{rand} \begin{pmatrix} \langle O_A \rangle [i-1] \\ \langle O_B \rangle [i-1] \end{pmatrix}, \quad (2)$$

where $\alpha \in \{0, 1\}$ is the mixture constant, W_{mix}^{rand} is a positive stochastic matrix that allows one to connect outputs from different reservoirs via a classical information channel. We denoted $\langle \hat{O}_p \rangle_i$ as the output signal at the discrete timestep i . To increase the performance of the QRs, one usually uses the temporal multiplexing technique¹ by performing K additional measurements in between the subsequent timesteps i and $i+1$ to get $\langle \hat{O}_p \rangle_{ik}$ (see also Fig. 1-(b)). In a special case of just two reservoirs (QR-A and QR-B), one can measure the following observable: $\hat{O}(\{l_a, l_b\}) = (\otimes_{a=1}^{n_A} \hat{Z}_a^{l_a}) \otimes (\otimes_{b=1}^{n_B} \hat{Z}_b^{l_b})$, where $\{l_a, l_b\} \in \{0, 1\}$. Note that usually a backaction of measurements on QR dynamics is not considered due to the possibility of performing simultaneous measurements some observable for a big ensemble of identical reservoirs (Fig.1). It is assumed for each timestep i that one has performed $i-1$ encoding steps which alternate with unitary evolution. One then begins to extract the output signal at timestep i (Fig.1 - c). In the present work, we consider the simplest form of the observable $\hat{O} \equiv \hat{\mathbf{I}}_A \otimes \hat{\mathbf{I}}_{B/\bullet} \otimes \hat{Z}_{(\bullet)}$, where $\hat{Z}_{(\bullet)}$ is an operator that acts on a Hilbert space of an arbitrary readout qubit of reservoir B , and $\hat{\mathbf{I}}$ is unit operator. Finally, the learning procedure with the QRC is straightforward. In the supervised learning setup, we have a training sequence as a function of a timestep i - $\mathbf{Y}[i]$. The objective is to minimize the mean square error (MSE):

$$\mathbf{W}_* = \underset{\mathbf{W}}{\text{argmin}} \|\mathbf{Y}_{train} - \mathbf{Y}_{mod.}(\mathbf{W})\|_2; \mathbf{Y}_{mod.}(\mathbf{W}) = \langle \mathbf{O} \rangle_{out} \mathbf{W}^T. \quad (3)$$

In Eq.(3) $\mathbf{Y}_{mod.}(\mathbf{W})$ is a linear model that weighs the set of output signals $\langle \mathbf{O} \rangle_{out} \equiv \{\langle \hat{O}_p \rangle_{ik}\}$, where ik is reshaped in one multi-index, $\|\bullet\|_2$ is euclidean norm. Dimensions (shapes) of the above matrices are as follows: $\mathbf{Y}_{train} - [T, L_{out}]$, $\langle \mathbf{O} \rangle_{out} - [T, KN_{total} + 1]$, and $\mathbf{W} - [L_{out}, KN_{total} + 1]$. Thus, to train \mathbf{W} one performs the Moore-Penrose pseudoinverse operation:

$$\mathbf{W}_*^T = (\langle \mathbf{Z} \rangle^T \langle \mathbf{Z} \rangle + \lambda \mathbf{I})^{-1} \langle \mathbf{Z} \rangle^T \mathbf{Y}_{train}, \quad (4)$$

where λ is a regularization term. For our simulations, we set the regularization term's value $\lambda \sim 10^{-10}$. The value of the regularization term plays an important role in the overall performance of QRC. Moreover, simulations of QRC are sensitive even to small numerical variations of the output signals. One needs to tune the regularization term to avoid misinterpretations of the QRC simulations results and prevent the QRC algorithm from overfitting. In the following section we consider a new QRC setup assisted by the bridge and purification channels and analyze its performance.

A setup of two quantum reservoirs assisted by the bridge channel

To demonstrate our approach based on an action of the bridge channel, we consider a quantum system of two uncorrelated QRs (subsystems QR-A and QR-B) at an initial timestep t . We use only a single qubit of the QR-A to encode the scalar signal in the QR system (Fig.2) via the standard encoding channel presented in the Eq.(1). The standard QRs dynamics, namely alternating action of encoding and unitary evolution channels, is now interrupted by the action of a bridge channel - nonselective projective measurements \mathcal{M}_b^a on two chosen qubits a from QR-A and b from QR-B (see Fig.(2) - (a)). The bridge channel \mathcal{M}_b^a acts once between two subsequent encoding procedures. The action of the bridge channel on arbitrary QR's state ρ_{AB} reads:

$$\hat{\rho}'_{AB} = \mathcal{M}_b^a[\hat{\rho}_{AB}] = \sum_{ij} \hat{\mathbf{I}}_{AB/a,b} \otimes \hat{\Pi}_{ij}^{(a,b)}(\vec{\theta}) \hat{\rho}_{AB} \hat{\mathbf{I}}_{AB/a,b} \otimes \hat{\Pi}_{ij}^{(a,b)}(\vec{\theta}), \quad (5)$$

where the operator $\hat{\Pi}_{ij}^{(a,b)}(\vec{\theta}) = \hat{U}(\vec{\theta}) |i_a j_b\rangle \langle i_a j_b| \hat{U}^\dagger(\vec{\theta})$, $i_a, j_b \in \{0, 1\}$ is the projective operator. Here we used standard notations $\{|i_a j_b\rangle\}$, $i_a, j_b \in \{0, 1\}$ for the two-qubit computational basis that in our case is transformed by the action of the unitary operator $\hat{U}(\vec{\theta})$. It allows one to parameterize a two-qubit basis used in nonselective measurements. We denoted $\vec{\theta}$ as the vector of parameters. Note that if the unitary operator $\hat{U}(\vec{\theta})$ is factorized as $\hat{U}(\vec{\theta}) = U_a(\vec{\theta}) \otimes U_b(\vec{\theta})$, the resulting two-qubit measurements basis cannot be used to "connect" (create correlations between) the reservoirs QR-A and QR-B. More details are provided in the **Methods** section. We used the following ansatz^{30,31} to represent arbitrary two-qubit operator $\hat{U}(\vec{\theta})$:

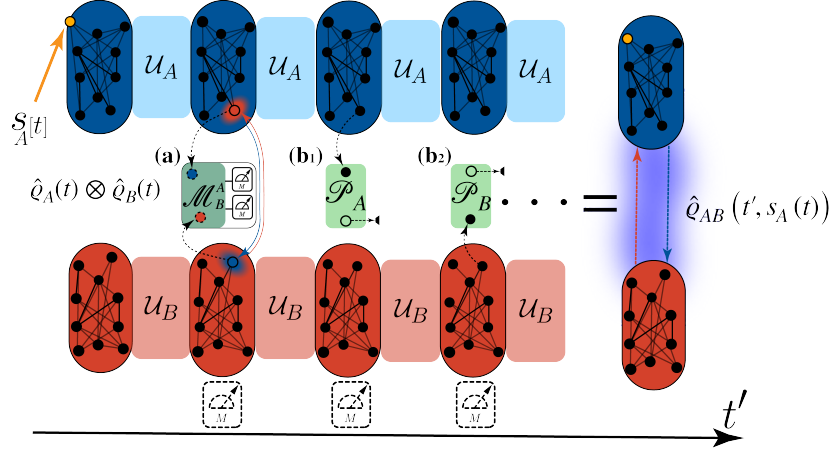


Figure 2. The schematics of the QR's dynamics assisted by the bridge channel \mathcal{M}_b^a - (a) for transmission of information from the QR's subsystem QR-A to the subsystem QR-B. It is implemented as nonselective measurements on two chosen qubits (bridge qubits): a from QR-A and b from QR-B. Auxiliary purification channels \mathcal{P}_A - (b1) and \mathcal{P}_B - (b2) subsequently act on the bridge qubits but separated by unitary evolution \mathcal{U}_A and \mathcal{U}_B driven by corresponding Hamiltonians. This alternation is necessary to spread the information inside each the QR's subsystems. Only one qubit in the QR-A is used for the signal encoding $S_A[t]$ (arrow with $S_A[t]$). At an initial timestep t , it is assumed that the QR state is factorized. The resulting state of the QR at some time t' is $\hat{\rho}_{AB}(t', S_A[t])$.

$$\hat{U}(\vec{\theta}) = \hat{U}_a(\theta_{1...3}) \otimes \hat{U}_b(\theta_{4...6}) e^{-i(\theta_7 \hat{X} \otimes \hat{X} + \theta_8 \hat{Y} \otimes \hat{Y} + \theta_9 \hat{Z} \otimes \hat{Z})} \hat{V}_a(\theta_{10...12}) \otimes \hat{V}_b(\theta_{13...15}). \quad (6)$$

The vector $\vec{\theta}$ in Eq.(6) contains fifteen parameters. Unitary operators $\{\hat{U}, \hat{V}\}_{a,b}$ are parameterized with three parameters each as standard qubit rotation operators along an arbitrary axis³². Using a heuristic optimization strategy, we derived the particular $\vec{\theta}_*$ that is utilized in our simulations (see the **Methods** section). It is important to demonstrate that QR's dynamics with the bridge channel can indeed transfer information from QR's subsystem QR-A to QR's subsystem QR-B. As a demonstration we analyze the performance of setups where we extract output information only from the QR-B varying numbers of qubits in QR-A and QR-B Fig.(3). We utilize the temporal multiplexing technique¹ in all further calculations, using $K = 10$ as our multiplexing parameter.

In general one can extract the output signal from each QR's qubit. For extraction output signals one performs multiple measurements of an observable over all ensemble for a chosen "extraction" qubit, including bridge's qubits a and b (see Fig. (1)). However, the action of the bridge channel severely affects the purity $P = \text{tr} \hat{\rho}_\bullet^2$ of any QR's subsystems states including states of a and b , which might worsen the QRC performance. In addition, to simulate the influence of noise on QR's dynamics, we introduce an action of the depolarization channel on each qubit (excluding qubits under action of a bridge channel) of the QR:

$$\Phi_{dp.}(p)[\bullet] = p/2 \hat{\mathbf{I}} + (1-p)[\bullet], \quad (7)$$

where $p \in [0, 1]$ - is the probability of depolarization for the chosen qubit. To circumvent this problem, we introduce an ancilla qubit system in a fiducial pure state $|0\rangle_a$. Interaction with an ancilla can be used to purify a particular single qubit subsystem³³. In our simulations, we deliberately assume that one has access only to the bridge qubits and only one encoding qubit in the QR's subsystem A. Thus, a purification channel acts on the bridge qubits a or b - Fig.(2) - (b1, b2) and can be written as follows:

$$\mathcal{P}_\bullet[\hat{\rho}_{AB}] = \text{tr} \left[\hat{\mathbf{I}}_{AB/\bullet} \otimes \hat{U}_\bullet(\gamma) \hat{\rho}_{AB} \otimes |0\rangle_{aa} \langle 0| \hat{\mathbf{I}}_{AB/\bullet} \otimes \hat{U}_\bullet^\dagger(\gamma) \right]. \quad (8)$$

We optimize the purification channel using the same ansatz for the unitary operator $\hat{U}_\bullet(\gamma)$ that was used to optimize the bridge channel Eq.(6), but the optimization heuristic is different. It is based on the trade-off between purity P of the particular qubit and the fidelity $F = \text{tr} \left(\sqrt{\sqrt{\hat{\rho}^{out}} \hat{\rho}^{in} \sqrt{\hat{\rho}^{out}}} \right)$ calculated for its state before and after purification. Based on the result of ansatz optimization, we indeed achieved a significant QRC performance improvement for different setups without depolarization Fig.(3) and with depolarization (compare Fig. (5) and Fig. (4)).

Finally, to quantify the performance of the proposed approaches, we focus on a commonly used QRC task - short-term memory task (STM)²¹. We analyze this task using several metrics. The first is memory accuracy $MA(d)$ ³⁴ given by

$$MA(d) = \frac{\text{cov}^2(\mathbf{Y}_{mod.}, \mathbf{Y}_{test.}(d))}{\text{var}(\mathbf{Y}_{mod.})\text{var}(\mathbf{Y}_{test.}(d))}, \quad (9)$$

where Y_{mod} is the prediction of QRC, and $Y_{test.}(d) = s[i-d]$ is the input signal, shifted by d steps. Symbols var , cov represent standard variance and covariance. We take a random binary signal as an input signal to the STM task. Secondly, to quantify the prediction accuracy, we calculate the euclidean length (the L_2 vector norm) of the prediction error: $\text{Gen.Loss} = \|\mathbf{Y}_{mod.} - \mathbf{Y}_{test.}\|_2$. We also analyze the negative of the first derivative of $MA(d)$. The maximum of this value allows to estimate the time interval where the generalization power drops significantly. This interval can therefore be treated as the memory length of a particular QR setup. Other metrics, such as the memory capacity $MC(d_{max}) = \sum_{d=0}^{d_{max}} MA(d)$, are also presented in the analysis of the setups where the output signal is extracted from both QR-A and QR-B.

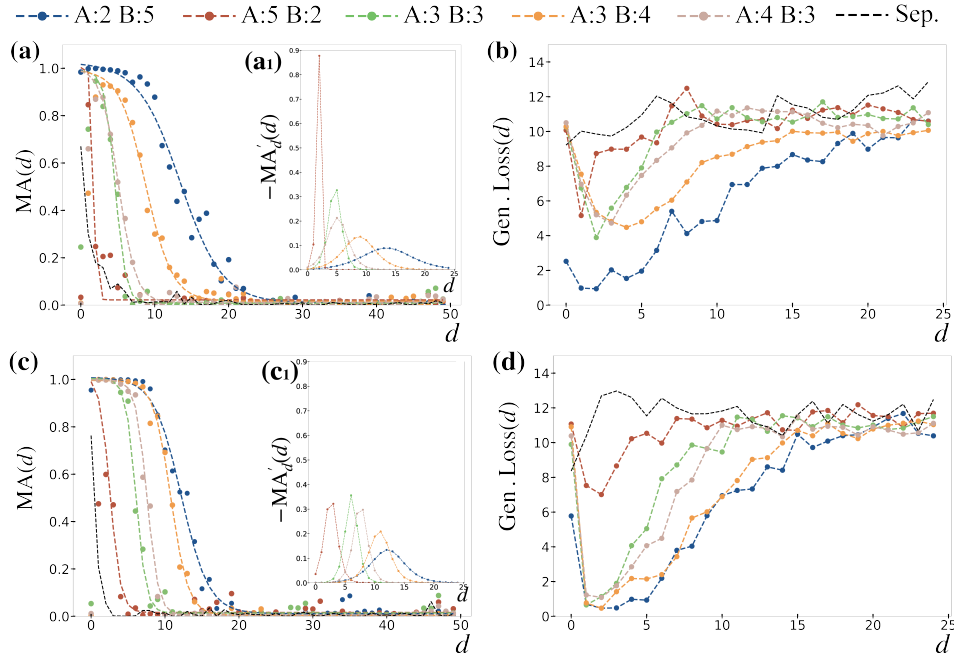


Figure 3. Top row: memory accuracy - **(a)**, it's derivative- **(a1)**, and the generalization loss - **(b)** with respect to the offset d in the STM task. The purification channel \mathcal{P} is switched off. Bottom row: same as top row with memory accuracy - **(c)**, it's derivative - **(c1)**, and the generalization loss - **(d)** but with the action of the purification channel \mathcal{P} . The channel \mathcal{P} is applied to the bridge qubits two times between any subsequent encoding operations. Different lines correspond to the setups with different numbers of qubits in subsystems QR-A and QR-B. The output signals are taken only from the QR-B to check the ability of the bridge channel to transfer the information. The timestep of unitary QR dynamics is different for each setup and is found experimentally. We chose the timestep that minimizes the sum of generalization losses for offsets from $d = 0$ to $d = 8$ in the STM task. The channel \mathcal{P} increases the performance in most setups. Generalization loss has a spike at $d = 0$. This effect stems from the fact that information spreading has a finite speed. It requires some time to propagate from the encoding qubit in QR-A to the readout qubits in QR-B. So most of the outputs from QR-B at timestep i have no information about the signal s_i . The case (Sep.) explicitly indicates that learning and generalization are impossible within the case of nonselective measurements along separable bases.

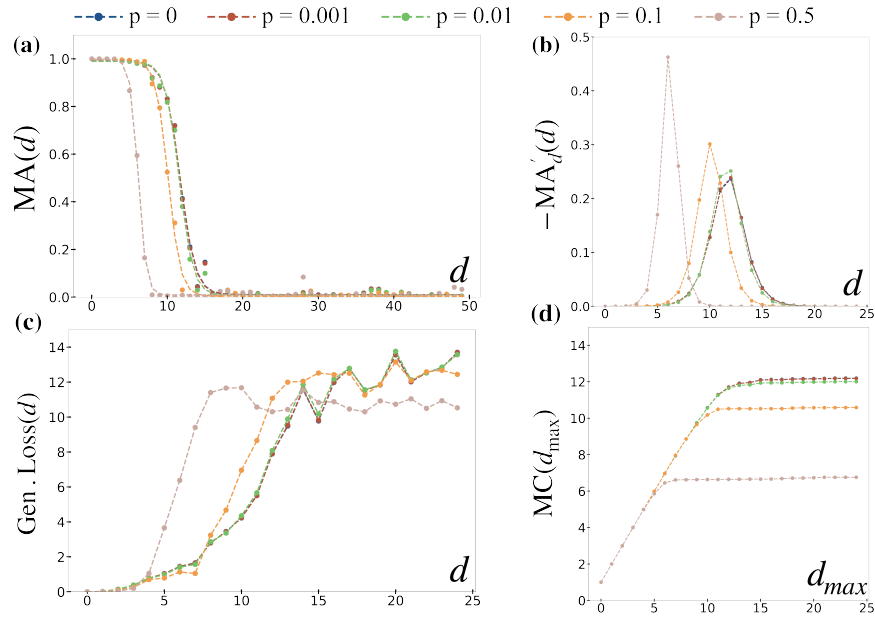


Figure 4. Memory accuracy (a), it's derivative (b), generalization loss (c), and memory capacity (d) for a setup with 3 qubits in QR-A and 4 qubits in QR-B. The system is affected by the depolarization of the form (7). Different lines correspond to different depolarization probabilities p . The purification channel is applied to the bridge qubits two times between any subsequent encoding operations. Output signals are taken from both QR-A and QR-B to check the total performance of the setup. Clearly, the system performance is stable against depolarization with probability up to $p = 0.1$.

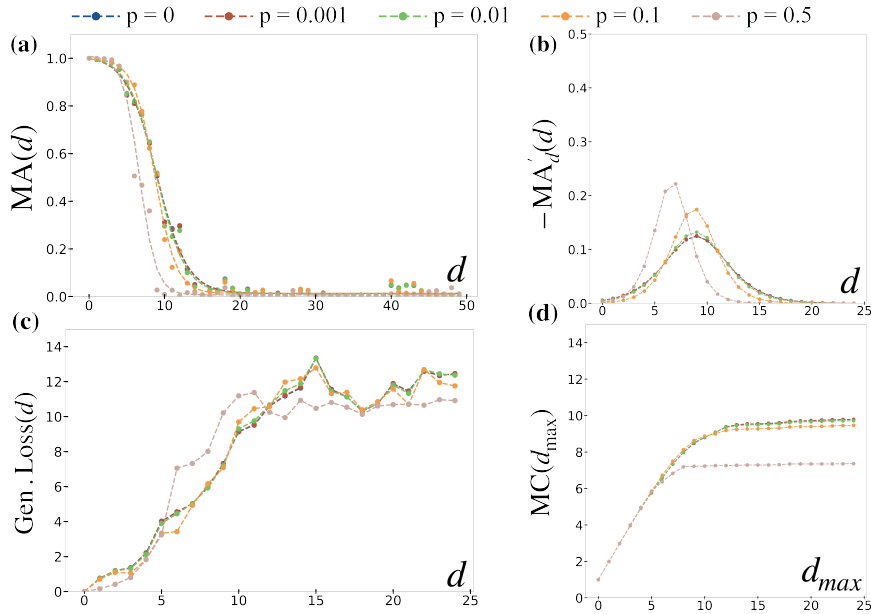


Figure 5. The metrics and setup are identical to Fig.4 but purification channel is not applied. In the most setups the action of purification channel can mitigate influence of depolarization (see Fig. 4).

In this section we demonstrated the usefulness of the auxiliary purification channels, we compared various setups with and without these channels in Fig.(3), Fig. (4), Fig. (5). Fig.(3) shows an STM task with the output signal gathered only from the subsystem B for various number of qubits. This figure evidently validates that the bridge channel can indeed be used to transfer quantum information between quantum reservoirs. Fig. (4) and Fig. (5) focus on the effect of depolarization on QRC performance. Finally, Fig. (6) explicitly demonstrates the performance of one chosen setup previously analyzed in Fig. (4).

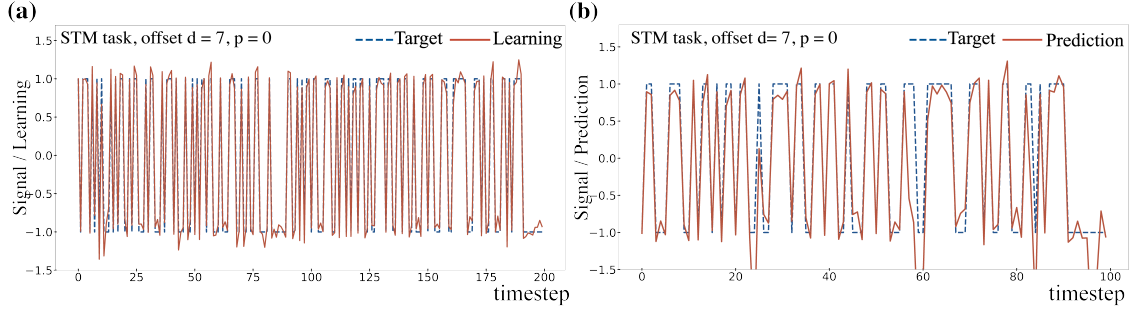


Figure 6. Visualization of the STM task performance on a random binary input signal for a setup with 3 qubits in QR-A and 4 qubits in QR-B. STM task offset $d = 7$ corresponds to a good memory accuracy (see Fig. 4). The left and right plots depict the performance of the algorithm on the training (a) and testing data (b) sets respectively. Depolarization is not taken into account ($p = 0$). The purification channel is applied to the bridge qubits two times between any subsequent encoding operation.

Summary

It is clear that due to practical limitations caused by control difficulties and a magnitude of noise in quantum systems, the accessible quantum-enhanced feature space of QR is also limited. In practice, the construction of relatively small QRs is one of the most realistic solutions that increase the scalability of QRC. In this paper, we suggested a novel way to connect QRs in a network. We proposed utilizing two-qubit nonselective measurements along an entangled basis to transfer information between QRs within the network. This channel, denoted as the bridge, allows one to make a network of reservoirs without any classical communication between them. The proposed approach excludes classical information processing for the QRC procedure up to the final linear optimization step. In addition, we introduced auxiliary single-qubit purification channels to further enhance QRC performance. Our approach can be treated as an intermediate scheme in-between QCL and QRC. This is clearly seen from the presented numerical optimization algorithm for both the bridge and the purification channels. Optimization algorithms are based on a specific channel's parametrization and the analysis of its matrix representation. Note that the optimization strategy is unconditional - it does not depend on a particular QRC task, its structure and does not require a lot of computational resources. Note that the optimization strategy can be potentially extended further by considering a particular QR structure.

We demonstrated the performance of two QRs connected via the bridge channel by numerical simulations. We observed that the optimized bridge channel with just 7 qubits produces memory accuracy comparable with a classically connected QRs network of 25 qubits. We use simulations to validate that the purification procedure enhances the QRC performance affected by noise.

Another possible performance enhancement could be achieved by the optimization of the channel application sequence by considering more than two-qubit subsystems. Generally, one could also analyze the number of bridge and purification channel applications between subsequent encoding operations. The particular parameters of the given QRC setup should be optimized for various physical QR realizations: photons, atoms, molecules, etc. The most important problem for further investigation is analyzing the performance and scalability of setups with more than two QRs, which is the next step of our research. We believe that subsequent development of a proposed technique and enhancements of optimization strategies will drastically increase the computational power of setups with an arbitrary number of interconnected QRs. As a result, adjustable QR networks will expand QRC applications, including classical and quantum information processing tasks.

Methods

In the main text, we proposed to use nonselective measurements Eq.(5) - bridge channel to transfer information between QR-A and QR-B. Additionally, to improve QRC performance, we utilize a purification channel Eq.(8). We use a general ansatz Eq.(6) to parametrize both quantum channels. In this section, we proposed heuristic optimization strategies for the given ansatz.

Let us start by considering the bridge channel. Firstly, it is easy to show explicitly that the "presence" of entanglement is necessary for information transfer via the bridge channel. We assumed that information about a signal is encoded in QR-A at arbitrary time t . Here for simplicity we implied that no information about a signal was presented in the QR system before time t . Thus, an arbitrary initial state (density operator) of QR after encoding can be written as follows:

$$\hat{\rho}_{AB}(t) = \sum_k q_k \hat{\rho}_{A/a,a}^{[k]}(s,t) \otimes \hat{\rho}_{b,B/b}^{[k]}(t). \quad (10)$$

In Eq.(10), a standard quantum state normalization is assumed $\sum_k q_k = 1$. Coefficients q_k do not depend on the encoded signal

and $\text{tr}_A \text{tr}_B(\hat{\rho}_{AB}(t)) = \text{tr}_B \text{tr}_A(\hat{\rho}_{AB}(t)) = 1$. If we put coefficients $\theta_7, \dots, \theta_9 \equiv 0$ in Eq.(6) and substitute it in Eq.(5), the resulting state after the action of the bridge channel $\hat{\rho}'_{AB}(t) = \mathcal{M}_b^a[\hat{\rho}_{AB}(t)]$ has the following form:

$$\hat{\rho}'_{AB}(t) = \sum_{i_a, j_b, k} q_k \left(\langle i_a | \hat{Q}_a \hat{\rho}_{A/a, a}^{[k]}(s, t) \hat{Q}_a^\dagger | i_a \rangle \right) | i_a \rangle \langle i_a | \otimes \left(\langle j_b | \hat{Q}_b \hat{\rho}_{B/b, b}^{[k]} \hat{Q}_b^\dagger | j_b \rangle \right) | j_b \rangle \langle j_b | = \sum_k q_k \hat{\rho}'_{A, a}^{[k]}(s, t) \otimes \hat{\rho}'_{B, b}^{[k]}(t), \quad (11)$$

where $\hat{Q}_{a,b} = \hat{U}_{a,b} \otimes \hat{V}_{a,b}$ - unitary operators act on subsystems a or b . Thus, for any observable $\hat{\mathbf{I}}_A \otimes \hat{O}_B$, the resulting mean value $\langle \hat{\mathbf{I}}_A \otimes \hat{O}_B \rangle$ does not carry any information about the encoded signal:

$$\langle \hat{\mathbf{I}}_A \otimes \hat{O}_B \rangle = \sum_k q_k \text{tr}_A(\hat{\rho}'_{A, a}^{[k]}(s, t)) \text{tr}_B(\hat{O}_B \hat{\rho}'_{B, b}^{[k]}(t)) = \sum_k q_k \text{tr}_B(\hat{O}_B \hat{\rho}'_{B, b}^{[k]}(t)). \quad (12)$$

Thereby nonselective measurements parametrized with $\theta_7, \dots, \theta_9 \equiv 0$ can not lead to information transfer between QR's subsystems. One can use a channel matrix representation to gain more insights about the structure of a bridge channel. As we briefly mentioned in the introduction, quantum channels are linear mappings on the vector space of the trace class operators²⁶. Let us fix an orthogonal operator basis set for the QR system: $\{\hat{\sigma}_a \otimes \hat{\sigma}_b \otimes \hat{e}_\xi\}$. Operators $\{\sigma_{a,b}; a, b \in \{0, \dots, 3\}\}$ are standard Pauli operators $\{\hat{\mathbf{I}}, \hat{X}, \hat{Y}, \hat{Z}\}$ acting on qubits a and b . Basis operators $\hat{e}_\xi, \xi_{0, \dots, 4(N_{total}-2)-1}$ act on subsystem QR-AB/ab. We explicitly distinguished basis operators corresponding to a subsystem of bridge qubits. Thus, we can also represent an arbitrary QR state $\hat{\rho}_{AB}(t)$:

$$\hat{\rho}_{AB}(t) = \sum_{ab, \xi} r_{ab, \xi}(t) (\hat{\sigma}_a \otimes \hat{\sigma}_b) \otimes \hat{e}_\xi; \quad r_{ab, \xi}(t) = \text{tr} \left(\hat{\rho}_{AB}(t) \frac{(\hat{\sigma}_a \otimes \hat{\sigma}_b)}{4} \otimes \frac{\hat{e}_\xi}{2^{N_{total}-2}} \right) \quad (13)$$

The action of an arbitrary two-qubit channel $\mathbf{I}_{AB/ab} \otimes \mathcal{Y}_b^a[\hat{\rho}_{AB}(t)]$ can be represented by:

$$\hat{\rho}'_{AB}(t) = \mathbf{I}_{AB/ab} \otimes \mathcal{Y}_b^a[\hat{\rho}_{AB}(t)] = \sum_{ab, \xi} r_{ab, \xi}(t) \mathcal{Y}_a^b[\hat{\sigma}_a \otimes \hat{\sigma}_b] \otimes \hat{e}_\xi = \sum_{ab, \xi} \left(\sum_{a'b', \xi'} \Upsilon_{ab, a'b'} \delta_{\xi, \xi'} r_{a'b', \xi'}(t) \right) (\hat{\sigma}_a \otimes \hat{\sigma}_b) \otimes \hat{e}_\xi, \quad (14)$$

where matrix $\Upsilon_{ab, a'b'}$ - is a matrix representation of a two-qubit channel $\mathcal{Y}_b^a[\bullet_{a,b}]$. It has the following form $\Upsilon_{ab, a'b'} = \frac{1}{4} \text{tr}(\hat{\sigma}_a \otimes \hat{\sigma}_b \mathcal{Y}_b^a[\hat{\sigma}_{a'} \otimes \hat{\sigma}_{b'}])$. As we mentioned earlier both bridge and purification channels depend on the same ansatz Eq.(6) which implies parametrization of a particular channel and its matrix representation on parameters θ : $\mathcal{Y}_b^a(\theta) \rightarrow \Upsilon_{ab, a'b'}(\theta)$. To optimize the bridge channel $\mathcal{M}_b^a(\theta)$ with corresponding matrix representation $M_{ab, a'b'}(\theta)$ we use the following heuristic observation. One can notice that in the case of nonselective measurements along separable bases (no entanglement presence in ansatz Eq.(6), Eq.(11)) a 1 - norm of the $M_{ab, a'b'}(\theta)$, in general, is less than in the case of measurements along entangled bases $\|M_{ab, a'b'}^{SEP}\|_1 \leq \|M_{ab, a'b'}^{ENT}\|_1$. By definition 1 - norm is the maximum absolute column sum of a matrix. From Fig.(7), it is clear why 1 - norm is a good candidate. Let us take a look at an arbitrary factorized two-qubit state $\hat{\rho}_{ab} = \hat{\rho}_a \otimes \hat{\rho}_b = \sum_{ab} r_a r_b (\hat{\sigma}_a \otimes \hat{\sigma}_b)$. The corresponding coefficients $r_a r_b$ in a matrix representation are also factorized. Let us assume that r_a is some function of a signal s : $r_a \equiv r_a(s)$ that carries some "valuable" information. Consequently, if one would like to transfer "valuable" information about a signal from a to b , one needs to "mix" corresponding coefficients and assemble a new non-factorized matrix r_{ab} . One also tends r_{ab} to have the maximum number of non-zero elements, which nontrivially depend on a signal. The diversity of transformations of valuable information inside a reservoir system is an essential feature of RC, both classical and quantum. Indeed, it means the matrix representation of a bridge channel has to be as "diverse" as possible. This observation can be directly verified via a plot of the matrix $M_{ab, a'b'}(\theta)$ for various cases (see Fig.7). It is clear that the bridge channel's matrix in the case of nonselective measurements along the entangled basis in Fig.(7) - (a) is the most diverse. We also tend to find such a matrix $M_{ab, a'b'}(\theta_*)$ that contains as many nonzero values as possible. Based on these observations, we decided to use the following optimization objective:

$$\vec{\theta}_* = \text{argmax}_{\vec{\theta}} \|M_{ab, a'b'}(\vec{\theta})\|_1; \quad \theta_7^2 + \theta_8^2 + \theta_9^2 \gg 0.001. \quad (15)$$

We attack optimization problem Eqs.(15) numerically. We apply Adam optimization algorithm²⁹ which is common for machine learning tasks, with slightly adjusted default parameters. As a result, we have found the following optimal parameters for ansatz Eq.(6) in accordance with Eq.(15): $\theta_7 = 0.208, \theta_8 = -0.267, \theta_9 = -0.291$. All other values of θ_* and code of optimization algorithms are presented in the GitHub repository³⁵.

Let us switch on to purification channels. Auxiliary purification channels $\mathcal{P}_{A,B}$ improve the accuracy of QRC affected by noise. Specifically, purification channels can reduce the number of required measurements (over QR's ensemble of identical systems) to extract output signals - the average values of some observables $\langle \hat{O}_\bullet \rangle(s)$. It follows from the intrinsic structure of the

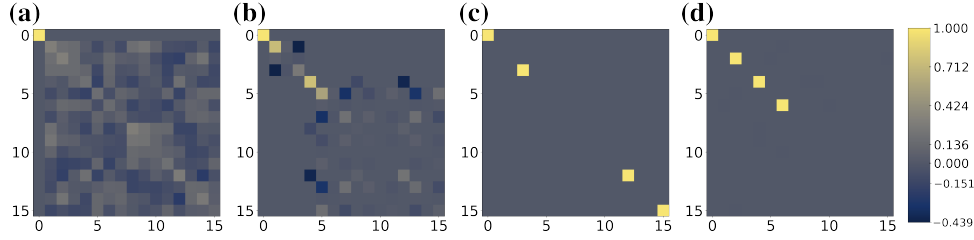


Figure 7. The figure presents a matrix plot of a bridge channel's matrix representation $M_{ab,a'b'}$. **(a)** - optimization results via optimization strategy described in Eq.(7). The corresponding matrix $M_{ab,a'b'}(\theta_*)$ is the most "diverse" and provides the best QRC performance of considered cases. **(b)** - matrix plot in the case of nonselective measurements along random separable basis with $(\theta_7 = \theta_8 = \theta_9 \equiv 0)$. **(c)** - matrix plot in the case of nonselective measurements along standard computational basis; the result corresponds to minimal $\|M_{ab,a'b'}^{SEP}\|_1 = 4$. **(d)** - results of "anti" optimization strategy where we minimize 1 - norm of a matrix $\|M_{ab,a'b'}\|_1$. In this case we have same values as in the case **(c)**: $\theta_{7*} = \theta_{8*} = \theta_{9*} \approx 0$ and minimal norm $\|M_{ab,a'b'}\|_1 \approx 4$. We verified optimization results **(c)** and **(d)** for various initial conditions for $\vec{\theta}$.

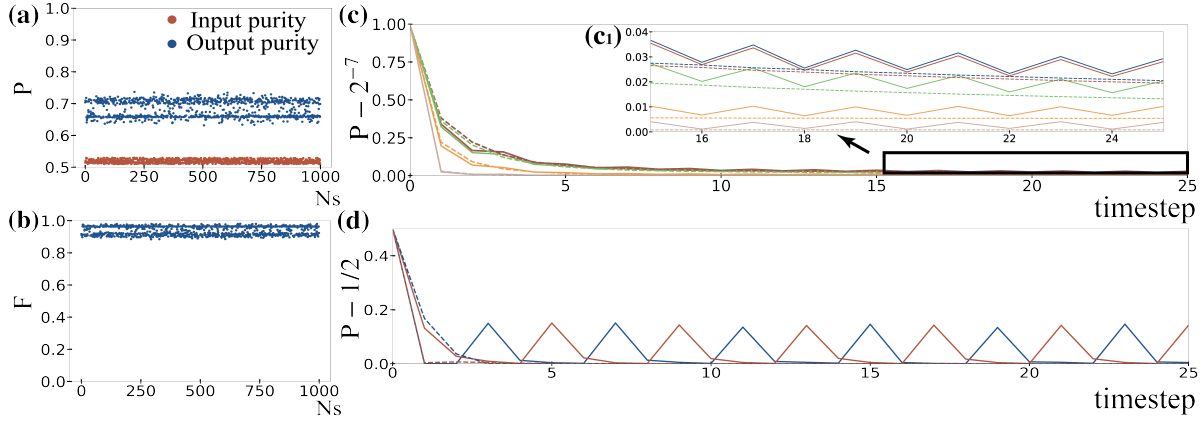


Figure 8. Results of numerical optimization for purification channel \mathcal{P} . We sampled 1000 qubit states with purity $P \in \{0.51, 0.53\}$ to verify optimization results. We observed a significant increase of P for corresponding output states - **(a)**, whilst fidelity F between input and output states is close to 0.9 - **(b)**. In the **(d)**, we presented results of the $\mathcal{P}(\gamma_*)$ channel's application to QR's bridge qubits; the depolarization parameter $p = 0$ in this case. The panel **(c)** shows purity for the full QR state $\hat{\rho}_{AB}$ affected by depolarization with parameters for the setup presented in the Fig.(4). We depicted both cases: with purification (solid lines) and without (dashed lines). In **(c)** and **(d)** we considered subsequent 25 timesteps of QRC dynamics with bridge and purification channels as depicted in Fig.(2).

QRC framework. Indeed, one addresses only to single corresponding qubit QR-"•" with the state $\hat{\rho}_\bullet = \text{tr}_{AB/\bullet}(\hat{\rho}_{AB})$ to perform measurements. Physically, it means that we have many identical measurement apparatuses that interact with corresponding QR's sub-ensemble. Alternatively, if we have just one QR system, we can prepare its state using the same sequence of operations multiple times to perform multiple measurement experiments. Thus, one derives output signals by estimating $\langle \hat{O}_\bullet \rangle (s) = \text{tr}_\bullet(\hat{\rho}_\bullet \hat{O}_\bullet)$ from statistics of measurements. It is clear that qubits states $\hat{\rho}_\bullet$ with purity $P = \text{tr}(\hat{\rho}_\bullet^2) \approx 1/2 + \varepsilon, \varepsilon \ll 1$ yield $\langle \hat{O}_\bullet \rangle (s) \approx \text{const} + \varepsilon \text{tr}(\hat{O}_\bullet |\Psi_\bullet(s)\rangle \langle \Psi_\bullet(s)|)$. Here the state $|\Psi_\bullet(s)\rangle \langle \Psi_\bullet(s)|$ is some pure state ($P_{|\Psi_\bullet(s)\rangle} \equiv 1$), const - a real number that does not depend on a signal. It means that the output signal carrying valuable information has a small magnitude $\sim \varepsilon$. Consequently it requires many measurements to recover a proper output signal. Purification can resolve this issue.

In the present work, we assume that we can only purify states of bridge qubits a and b . Without loss of generality we consider qubit a . To optimize purification channels $\mathcal{P}_{A,B}(\vec{\gamma})$ presented in Eq.(8) we again address to its matrix representations. We use the same parametrization ansatz $\hat{U}(\vec{\gamma})$ - Eq.(6) as we used before in the case of bridge optimization. A single qubit state has well-known geometrical representation on a Bloch sphere^{26,32}: $\hat{\rho}_a = (1/2)(\hat{\mathbf{I}} + \sum_a r_a \hat{\sigma}_a)$. Where \vec{r} is three dimensional euclidean vector such that $0 \leq \|\vec{r}\| \leq 1, \|\vec{r}\| = \sqrt{(\vec{r}, \vec{r})}$. Purity of state $\hat{\rho}_a$ is given by $P = (1/2)(1 + \|\vec{r}\|^2)$. The action of a purification channel results transformation of \vec{r} in accordance with:

$$\vec{r}' = \vec{q} + \Gamma \vec{r}; q_i = \frac{1}{2} \text{tr}(\hat{\sigma}_i \mathcal{P}(\vec{\gamma})[\mathbf{I}]), \Gamma_{ij} = \frac{1}{2} \text{tr}(\hat{\sigma}_i \mathcal{P}(\vec{\gamma})[\hat{\sigma}_j]); i, j \in \{1, 2, 3\}. \quad (16)$$

The optimization heuristic is straightforward. We aim to maximally increase the state's Purity and simultaneously preserve as much information as we can. As a measure of information "preservation", we use a Fidelity^{26,32}: $F = \text{tr} \left(\sqrt{\sqrt{\hat{\rho}_a} \hat{\rho}_a \sqrt{\hat{\rho}_a}} \right)$ between qubit's states before and after purification. Finally, we present $\mathcal{P}(\gamma)$ an optimization objective based on described above geometrical interpretation and Purity - Fidelity trade-off. As a result we choose the following form for the optimization objective:

$$\vec{\gamma}_* = \underset{\gamma}{\text{argmin}} \left| \frac{\|\Gamma^T(\gamma)\Gamma(\gamma)\|_F}{\|\vec{q}_\gamma\|} - 1 \right| \quad (17)$$

We denoted $\|\bullet\|_F$ in Eq.(17) a Frobenius norm of a matrix. Fig.(8) demonstrates the effectiveness of the proposed numerical optimization. Note, the trade-off between purity and fidelity in a state purification protocol via sampling methods was explored in work³⁶. As we mentioned we use the same numerical approach presented in the bridge channel optimization in our case. An application of Adam optimizer yields the following values $\gamma_7 = 0.44$, $\gamma_8 = 1.13$, $\gamma_9 = 0.44$. Other values of $\vec{\gamma}_*$ and code of optimization algorithms are presented in ours GitHub repository³⁵. We utilized the derived parameters γ_* in the **Results** to verify usefulness of a purification channel $\mathcal{P}(\gamma_*)$.

References

1. Fujii, K. & Nakajima, K. Harnessing disordered-ensemble quantum dynamics for machine learning. *Phys. Rev. Appl.* **8**, 024030, DOI: [10.1103/PhysRevApplied.8.024030](https://doi.org/10.1103/PhysRevApplied.8.024030) (2017).
2. Nakajima, K. & Fischer, I. (eds.) *Reservoir Computing* (Springer Singapore, 2021).
3. Cory, D. *et al.* NMR based quantum information processing: Achievements and prospects. *Fortschritte der Physik* **48**, 875–907, DOI: [10.1002/1521-3978\(200009\)48:9/11<875::aid-prop875>3.0.co;2-v](https://doi.org/10.1002/1521-3978(200009)48:9/11<875::aid-prop875>3.0.co;2-v) (2000).
4. Negrevergne, C. *et al.* Benchmarking quantum control methods on a 12-qubit system. *Phys. Rev. Lett.* **96**, 170501, DOI: [10.1103/PhysRevLett.96.170501](https://doi.org/10.1103/PhysRevLett.96.170501) (2006).
5. Ryan, C. A., Laforest, M. & Laflamme, R. Randomized benchmarking of single- and multi-qubit control in liquid-state NMR quantum information processing. *New J. Phys.* **11**, 013034, DOI: [10.1088/1367-2630/11/1/013034](https://doi.org/10.1088/1367-2630/11/1/013034) (2009).
6. Jones, J. A. Quantum computing with NMR. *Prog. Nucl. Magn. Reson. Spectrosc.* **59**, 91–120, DOI: [10.1016/j.pnmrs.2010.11.001](https://doi.org/10.1016/j.pnmrs.2010.11.001) (2011).
7. Schütz, M. J. *Quantum dots for quantum information processing: Controlling and Exploiting the Quantum Dot Environment* (Springer, 2016).
8. Georgescu, I. M., Ashhab, S. & Nori, F. Quantum simulation. *Rev. Mod. Phys.* **86**, 153–185, DOI: [10.1103/RevModPhys.86.153](https://doi.org/10.1103/RevModPhys.86.153) (2014).
9. Mujal, P. *et al.* Quantum reservoir computing in bosonic networks. In Volpe, G., Pereira, J. B., Brunner, D. & Ozcan, A. (eds.) *Emerging Topics in Artificial Intelligence (ETAI) 2021*, DOI: [10.1117/12.2596177](https://doi.org/10.1117/12.2596177) (SPIE, 2021).
10. Nokkala, J. *et al.* Gaussian states of continuous-variable quantum systems provide universal and versatile reservoir computing. *Commun. Phys.* **4**, DOI: [10.1038/s42005-021-00556-w](https://doi.org/10.1038/s42005-021-00556-w) (2021).
11. Ghosh, S., Paterek, T. & Liew, T. C. H. Quantum neuromorphic platform for quantum state preparation. *Phys. Rev. Lett.* **123**, 260404, DOI: [10.1103/PhysRevLett.123.260404](https://doi.org/10.1103/PhysRevLett.123.260404) (2019).
12. Ghosh, S., Opala, A., Matuszewski, M., Paterek, T. & Liew, T. C. H. Reconstructing quantum states with quantum reservoir networks. *IEEE Transactions on Neural Networks Learn. Syst.* 1–8, DOI: [10.1109/TNNLS.2020.3009716](https://doi.org/10.1109/TNNLS.2020.3009716) (2020).
13. Ghosh, S., Opala, A., Matuszewski, M., Paterek, T. & Liew, T. C. H. Quantum reservoir processing. *npj Quantum Inf.* **5**, DOI: [10.1038/s41534-019-0149-8](https://doi.org/10.1038/s41534-019-0149-8) (2019).
14. Tran, Q. H. & Nakajima, K. Learning temporal quantum tomography. *arXiv preprint arXiv:2103.13973* (2021).
15. Killoran, N. *et al.* Continuous-variable quantum neural networks. *Phys. Rev. Res.* **1**, 033063, DOI: [10.1103/PhysRevResearch.1.033063](https://doi.org/10.1103/PhysRevResearch.1.033063) (2019).
16. Mitarai, K., Negoro, M., Kitagawa, M. & Fujii, K. Quantum circuit learning. *Phys. Rev. A* **98**, DOI: [10.1103/physreva.98.032309](https://doi.org/10.1103/physreva.98.032309) (2018).
17. McClean, J. R., Boixo, S., Smelyanskiy, V. N., Babbush, R. & Neven, H. Barren plateaus in quantum neural network training landscapes. *Nat. Commun.* **9**, DOI: [10.1038/s41467-018-07090-4](https://doi.org/10.1038/s41467-018-07090-4) (2018).

18. Schuld, M. & Killoran, N. Quantum machine learning in feature hilbert spaces. *Phys. Rev. Lett.* **122**, 040504, DOI: [10.1103/PhysRevLett.122.040504](https://doi.org/10.1103/PhysRevLett.122.040504) (2019).
19. Schuld, M., Sinayskiy, I. & Petruccione, F. An introduction to quantum machine learning. *Contemp. Phys.* **56**, 172–185, DOI: [10.1080/00107514.2014.964942](https://doi.org/10.1080/00107514.2014.964942) (2014).
20. Nakajima, K., Fujii, K., Negoro, M., Mitarai, K. & Kitagawa, M. Boosting computational power through spatial multiplexing in quantum reservoir computing. *Phys. Rev. Appl.* **11**, 034021, DOI: [10.1103/PhysRevApplied.11.034021](https://doi.org/10.1103/PhysRevApplied.11.034021) (2019).
21. Kutvonen, A., Fujii, K. & Sagawa, T. Optimizing a quantum reservoir computer for time series prediction. *Sci. Reports* **10**, DOI: [10.1038/s41598-020-71673-9](https://doi.org/10.1038/s41598-020-71673-9) (2020).
22. Tran, Q. H. & Nakajima, K. Higher-order quantum reservoir computing. *arXiv preprint arXiv:2006.08999* (2020).
23. Lu, D. *et al.* Enhancing quantum control by bootstrapping a quantum processor of 12 qubits. *npj Quantum Inf.* **3**, 1–7 (2017).
24. Luchnikov, I. A., Vintskevich, S. V., Grigoriev, D. A. & Filippov, S. N. Machine learning non-markovian quantum dynamics. *Phys. Rev. Lett.* **124**, 140502, DOI: [10.1103/PhysRevLett.124.140502](https://doi.org/10.1103/PhysRevLett.124.140502) (2020).
25. Luchnikov, I. *et al.* Probing non-markovian quantum dynamics with data-driven analysis: Beyond "black-box" machine learning models. *arXiv preprint arXiv:2103.14490* (2021).
26. Heinosaari, T. & Ziman, M. *The Mathematical language of Quantum Theory* (Cambridge University Press, 2009).
27. Kalev, A., Mann, A. & Revzen, M. Choice of measurement as the signal. *Phys. Rev. Lett.* **110**, 260502, DOI: [10.1103/PhysRevLett.110.260502](https://doi.org/10.1103/PhysRevLett.110.260502) (2013).
28. Zuppardo, M., Ganardi, R., Miller, M., Bandyopadhyay, S. & Paterek, T. Entanglement gain in measurements with unknown results. *Phys. Rev. A* **99**, 042319, DOI: [10.1103/PhysRevA.99.042319](https://doi.org/10.1103/PhysRevA.99.042319) (2019).
29. Kingma, D. P. & Ba, J. Adam: A method for stochastic optimization. *arXiv preprint arXiv:1412.6980* (2014).
30. Guan, Z. *et al.* Entangling power of two-qubit gates on mixed states. *Phys. Rev. A* **89**, 012324, DOI: [10.1103/PhysRevA.89.012324](https://doi.org/10.1103/PhysRevA.89.012324) (2014).
31. Kraus, B. & Cirac, J. I. Optimal creation of entanglement using a two-qubit gate. *Phys. Rev. A* **63**, 062309, DOI: [10.1103/PhysRevA.63.062309](https://doi.org/10.1103/PhysRevA.63.062309) (2001).
32. Nielsen, M. A. & Chuang, I. L. *Quantum Computation and Quantum Information* (Cambridge University Press, 2009).
33. Cirac, J. I., Ekert, A. K. & Macchiavello, C. Optimal purification of single qubits. *Phys. Rev. Lett.* **82**, 4344–4347, DOI: [10.1103/PhysRevLett.82.4344](https://doi.org/10.1103/PhysRevLett.82.4344) (1999).
34. Jaeger, H. Short term memory in echo state networks. gmd-report 152. In *GMD-German National Research Institute for Computer Science (2002)*, <http://www.faculty.jacobs-university.de/hjaeger/pubs/STMEchoStatesTechRep.pdf> (Citeseer, 2002).
35. GitHub. Quantum reservoir computing assisted by nonselective measurements along entangled basis: Source code for numerical calculations. <https://github.com/StephenVintskevich/qRC> (2021).
36. Di Franco, C. & Paternostro, M. A no-go result on the purification of quantum states. *Sci. Reports* **3**, 1387, DOI: [10.1038/srep01387](https://doi.org/10.1038/srep01387) (2013).

Acknowledgements

This work is supported by the Russian Science Foundation under Project No. 20-72-00116. We thank Savva Morozov, Andrei Nomerotski and Andrey Rogachev for fruitful discussions and support.

Author contributions statement

Both authors contributed equally to the paper.

Additional information

Competing interests The authors declare no competing financial interests.